Sound velocities and thermodynamical properties of hcp iron at high pressure and temperature

Johann Bouchet, Francois Bottin, Daniele Antonangeli, Guillaume Morard

Sound velocities and thermodynamical properties of hcp iron at high pressure and temperature

Sound velocities and thermodynamical properties of hcp iron at high pressure and temperature

J. Bouchet[1,2], F. Bottin[2], D. Antonangeli[3], and G. Morard[3,4]

[1] CEA, DES, IRESNE, DEC F-13108 Saint-Paul-Lez-Durance, France.

[2] CEA, DAM, DIF, F-91297 Arpajon, France, and Université Paris-Saclay, CEA, Laboratoires des Matériaux en Conditions Extreêmes, 91680 Bruyères-le-Châtel, France.

[3]Sorbonne Université, Muséum National d'Histoire Naturelle, UMR CNRS 7590, Institut de Minéralogie, de Physique des Matériaux et de Cosmochimie, IMPMC, 75005 Paris, France

[4] Université Grenoble Alpes, CNRS, IRD, IFSTTAR, ISTerre, Grenoble, 38000, France

Abstract. Sound velocities and thermodynamical properties of hcp iron have been computed using *ab initio* calculations over an extended density and temperature range, encompassing the conditions directly relevant for the Earth's inner core. At room temperature, and up to 350 GPa, an excellent agreement is obtained between present results and experimental data for many thermodynamical quantities: phonon density of states, vibrational entropy, heat capacity, Grüneisen parameter and thermal expansion. With increasing temperature, along an isochore, we observe a strong decrease of the phonon frequencies, demonstrating that intrinsic anharmonic effects cannot be neglected. We also carefully compare previous theoretical data for the sound velocities and try to explain the discrepancies observed with experiments. Finally, we propose a temperature dependant Birch's law that we compare with previous experimental work.

Submitted to: *J. Phys.: Condens. Matter*

1. Introduction

Due to its technological and geophysical importance, iron is one of the most studied element of the periodic table. A large experimental effort has been devoted to the measure of its thermodynamical properties at pressures and temperatures relevant to Earth's interior. Among these properties the sound velocities [1, 2, 3, 4, 5] are key quantities since they can be directly related to seismological observations [6, 7]. Probing matter at such thermodynamical conditions ($\sim$ 330 GPa, $\sim$ 6000 K) is extremely challenging and in fact constraints are obtained by extrapolationof data at lower pressures and temperatures. In parallel to these experimental works and to circumvent the experimental limits, *ab initio* calculations have been performed to obtain

sound velocities [8, 9, 10, 11, 12]. In addition, other thermodynamical properties as thermal expansion or Grüneisen parameter have been calculated [13, 14, 15] to build reliable equation of state (EOS) and compare to experimental data [16, 5, 17].

Calculations at high pressure with density functional theory (DFT) can be performed simply by changing the value of the volume. Including temperature is a longstanding task, much more complex. Many approximations have been made, mostly based on the harmonic approximation, to indirectly simulate the temperature and describe the thermal behaviour of physical quantities. One of the best known is the quasi-harmonic approximation (QHA) [18] which introduces an implicit temperature dependence of the phonon frequencies and leads to a non-zero thermal expansion. The QHA is easy to implement and only requires 0 K calculations [14]. However, its temperature range of validity is difficult to assess and can strongly depend on the materials under consideration, since it is now well established that anharmonic effects, beyond the QHA, can be important far below the melting temperature [19, 20, 21].

In the past ten years, strong efforts have been made to take into account explicit temperature effects and go beyond the QHA. New methods capturing the thermal properties of solids at non-zero temperature are now available and can be applied in *ab initio* calculations. These approaches combine ideas including finite large displacements, molecular dynamics sampling, self consistent harmonic theories, and different force fitting schemes. The most widely used methods include Self-Consistent Ab Initio Lattice Dynamics (SCAILD) [22], Stochastic Self-Consistent Harmonic Approximation (SSCHA) [23, 24], Temperature Dependent Effective Potential (TDEP) [25, 26, 27], Anharmonic LAttice MODEl (ALAMODE) [28] and Compressive Sensing Lattice Dynamics [29]. Other methods obtain anharmonic contributions via thermodynamic integration [30], or a series expansion of the interatomic forces constants [31]. A large number of new phenomena, intrinsically temperature dependent, can now be captured: the modification of the phonon density of states (vDOS) and free energy, the (T, P) phase transition boundaries [32], the evolution of elastic constants [33] or Grüneisen coefficients, the phonon lifetimes [34], mechanisms behind superconductivity in pressure-stabilized hydrides [35] or the thermal conductivity [36].

In this paper we perform *ab initio* molecular dynamics (AIMD) simulations and

use the TDEP method to calculate the vibrational properties of iron up to pressure and temperature relevant for the Earth's core. In the next two sections we give the details of the calculations and the different equations used to calculate various physical quantities. Then we present results for the thermodynamical properties in section 4 and for the sound velocities in section 5 with careful comparison with previous theoretical and experimental data.

2. Computational Details

Ab initio simulations were performed using the ABINIT package [37, 38, 39] in the framework of the Projector Augmented Wave (PAW) method [40, 41]. We employ the generalized gradient approximation (GGA) according to the parametrization of Perdew, Burke and Ernzerhof (PBE) for the exchange-correlation energy and potential [42]. Using ATOMPAW [43, 44, 45], we generate a small core PAW atomic data with a radius r_{PAW} equal to 2.0 u.a, with $3s$, $3p$, $3d$, and $4s$ states as valence electrons and a cutoff energy equal to 350 eV for the plane wave basis set.

The simulation box includes 180 atoms and corresponds to a $5 \times 3 \times 3$ supercell of a 4-atoms C-centered orthorhombic cell (hcp structure with orthogonal axes). A good integration of electronic quantities is fulfilled using a $2 \times 2 \times 2$ Monkhorst–Pack mesh leading to the inclusion of 4 special **k**-points in the calculations. The size of the supercell and the **k**-points mesh used in present calculations give an uncertainty of less than 1% on the velocity, which cannot be obtained using smaller supercells (128 and 144 atoms) whatever the **k**-points mesh used (Γ point or $3 \times 3 \times 3$).

Tens of AIMD simulations are performed in the NVT ensemble (constant number of particles, constant volume and temperature) and are run for about 3-5 ps using a time step (τ) of 1.13 fs. In particular, AIMD simulations are carried out for five densities ρ equal to 10, 10.8, 12, 13.15 and 14 g.cm^{-3} corresponding to pressures between 50 and 350 GPa, and several temperatures from 300 up to 7000 K depending on the density considered. The brodening of the occupation numbers was beased on the Fermi-Dirac statistics with the electronic temperature equal to the ionic one. Taking benefit of an efficient scheme of parallelization [46] and using hundreds to thousands of processors, the recovery time is a few months.

3. Calculations of thermodynamic properties and sound velocities

To obtain dynamic, elastic and thermodynamic properties as a function of the temperature we used the TDEP approach developed by Hellman and coworkers [25, 26] and implemented in ABINIT [47, 27] as ATDEP. In this method, a model Hamiltonian expanded as a function of the atomic displacements around equilibrium and truncated at the second or third order is adjusted to fit the potential energy surface obtained using molecular dynamic simulations at finite temperature. As a results, we obtain the *effective* interatomic force constants (IFC) at the second $\Phi_{ij}^{\alpha\beta}(T)$ and third $\Psi_{ijk}^{\alpha\beta\gamma}(T)$

order, between i, j, k atoms and for any α, β, γ directions. These *effective* IFC are no longer constant as a function of the temperature but now depend on it.

By performing a Fourier transform of the *effective* 2^{nd} order IFC, we can get the dynamical matrix, the eigenvectors $X_{is}^{\alpha}(\mathbf{q}, T)$ and eigenvalues (phonon frequencies) $\omega_s(\mathbf{q}, T)$ at any $\mathbf{q}$-point of the Brillouin zone and for each phonon mode s. In addition, ATDEP provides the vDOS $g(\omega, T)$ and the associated thermodynamic properties: the specific heat $C_V(T)$, the vibrational entropy $S_{vib}(T)$, the vibrational energy $U_{vib}(T)$ and the vibrational free energy $F_{vib}(T)$.

Another thermodynamic quantity which can be derived from the IFCs is the Grüneisen parameter $\gamma = V\left(\frac{\partial P}{\partial U}\right)_V$, where U is the internal energy. For iron at Earth's inner core conditions, its determination is essential because it provides the link between the thermal pressure P_{vib} and the temperature (at high temperature, in the classical limit, $U_{vib}(T) = 3Nk_BT$, with k_B the Boltzmann constant). Consequently, this parameter is a key quantity for the Earth's interior where P_{vib} as a function of depth is well constrained, thanks to seismological data, but T is poorly known. The evolution of $\gamma(\rho, T)$ with density ρ, but also with temperature is therefore essential to build reliable equation of states (EOS) for planetary modeling [48, 49].

The mode Grüneisen parameters are defined by the volume derivatives of the phonon-mode frequencies:

$$\gamma_s(\mathbf{q}, T) = -\frac{V}{\omega_s(\mathbf{q}, T)}\left(\frac{\partial \omega_s(\mathbf{q}, T)}{\partial V}\right)_T \tag{1}$$

These later can be obtained [27] from the *effective* 3^{rd} order IFC $\Psi_{ijk}^{\alpha\beta\gamma}(T)$ as follows:

$$\begin{aligned}\gamma_s(\mathbf{q}, T) = & -\frac{1}{6\omega_s^2(\mathbf{q}, T)}\sum_{ijk\alpha\beta\gamma}\Psi_{ijk}^{\alpha\beta\gamma}(T) \\ & \times \frac{X_{is}^{\star\alpha}(\mathbf{q}, T)X_{js}^{\beta}(\mathbf{q}, T)}{\sqrt{M_iM_j}} r_k^{\gamma}\exp\left[i\mathbf{q}.\mathbf{R}_j\right]\end{aligned} \tag{2}$$

where M_i is the mass, r_i^{α} the vector position of atom i along α and $\mathbf{R}_i$ the lattice vector of the unitcell of atom i. From the mode Grüneisen parameters $\gamma_s(\mathbf{q}, T)$, the thermodynamical Grüneisen parameter writes:

$$\gamma(T) = \sum_{s=1}^{3N_a}\sum_{\mathbf{q}\in BZ}\frac{\gamma_s(\mathbf{q}, T)C_{V,s}(\mathbf{q}, T)}{C_V(T)} \tag{3}$$

where the $C_{V,s}(\mathbf{q}, T)$ are the mode heat capacities such as $C_V(T) = \sum_{s=1}^{3N_a}\sum_{\mathbf{q}\in BZ} C_{V,s}(\mathbf{q}, T)$ and BZ is the Brillouin zone.

As previously performed for the Grüneisen parameter, we can also obtain the temperature dependence of the isothermal elastic constants by using the *effective* 2^{nd} IFC and the formulation proposed in Refs. [50, 51, 33]:

$$C_{\alpha\beta\gamma\delta}(T) = A_{\alpha\gamma\beta\delta}(T) + A_{\beta\gamma\alpha\delta}(T) - A_{\alpha\beta\gamma\delta}(T) \tag{4}$$

with,

$$A_{\alpha\beta\gamma\delta}(T) = \frac{1}{2V}\sum_{ij}\Phi_{ij}^{\alpha\beta}(T)d_{ij}^{\gamma}d_{ij}^{\delta} \tag{5}$$

where d_{ij}^{α} is the distance between the atom i and j along α. The full isothermal elastic tensor $C_{\alpha\beta\gamma\delta}(T)$ can be reduced following the symmetries and the Voigt notation. The temperature effects are then directly introduced in the elastic constants by the temperature variation of the IFCs.

Once the $C_{\alpha\beta}(T)$ are obtained, the isothermal incompressibility $K_T(T)$ and the shear modulus $G(T)$ are given using the Voigt average for the hcp structure by:

$$K_T(T) = \frac{2(C_{11}+C_{12})+4C_{13}+C_{33}}{9} \tag{6}$$

$$G(T) = \frac{7C_{11}-5C_{12}+2C_{33}-4C_{13}+12C_{44}}{30} \tag{7}$$

We have also calculated K_T and G using the Reuss and Hill formulas, the differences were less than 0.3% compared to the Voigt average. From the Grüneisen parameter, the isothermal compressibility $\beta_T(T) = \frac{1}{K_T(T)}$ and the heat capacity, it is also possible to compute the thermal expansion of the system, with all the intrinsic and extrinsic thermal effects:

$$\alpha(T) = \frac{\gamma(T)C_V(T)}{\beta(T)V} \tag{8}$$

Finally, the adiabatic incompressibility $K_S(T)$, the compressional $V_P(T)$ and shear $V_S(T)$ velocities are obtained using all the previous results coming from the 2^{nd} and 3^{rd} orders, as follows:

$$K_S(T) = K_T(T)\Big(1+\alpha(T)\gamma(T)T\Big) \tag{9}$$

$$V_P(T) = \sqrt{\frac{K_S(T)+4/3G(T)}{\rho}} \tag{10}$$

$$V_S(T) = \sqrt{\frac{G(T)}{\rho}} \tag{11}$$

This procedure enables us to take into account the anharmonic effects not included in the QHA where only *implicit* effects coming from the thermal dilation is considered. This missing *explicit* anharmonic part, also called intrinsic, can be crucial for finite temperature elasticity, as shown on TiAlN alloys [33].

For comparison, the procedure to obtain the $C_{\alpha\beta}$ with the QHA [52, 14] is very tedious since the phonon spectra has to be calculated not only for the parent structure but also for all the strained structures with different values for the applied strain. So between 20 to 30 first principles linear-response calculations are necessary at each volume. Note that if the internal degree of freedom are relaxed for the strain structures at 0 K, their temperature dependency is not taken into account with this procedure.

Similar criticisms can be made for the method where the strains are applied to supercells [9, 53, 10]. At least 10 AIMD simulations are necessary with running time around 10 ps [10], resulting in an overall simulation time of 100 ps to obtain the set of elastic constants of the hcp structure at one thermodynamic point. By comparison, using TDEP, we obtain the elastic constants with a single simulation of about 5 ps. The main drawback of this method is that since the elastic constants are related to phonon frequencies in the long wavelenght limit, it requires large supercells to converge the sum in Eq. (5). To circumvent this difficulty, we only retain the temperature dependence of Eq. (4) that we apply to the static calculations at 0 K [33, 32].

4. Thermodynamic properties of ϵ-Fe

4.1. Phonon spectrum, phonon density of state and related quantities

As a first illustration, we compare in Figure 1 the vDOS obtained in present AIMD calculations at room temperature to the results obtained in nuclear resonant inelastic X-ray scattering (NRIXS) measurements on isotopically enriched ^{57}Fe [54](we consider natural ^{56}Fe in present calculations). The excellent agreement obtained attests the validity of vDOS computed as a function of the pressure (between 50 and 150 GPa) at low temperature and assess the quality of present calculations at higher pressure and temperature where no experimental data are available.

The phonon dispersion relations and the associated vDOS of hcp Fe at 13.06 g.cm^{-3} as a function of temperature are presented in Fig. 2. First, we do not observe any dynamical instabilities for the hcp structure even at 7000 K, a temperature close to the melting point (*ab initio* calculations evaluate the melting temperature around 6300 K at this density [56, 57] but the solid state can be maintained at higher temperature due to the overheating effect [15]). Secondly, we observe that the frequencies soften with temperature but not with the same amplitude. Up to 5000 K the temperature effect is rather small for the longitudinal branches (acoustic and optic) while we observe a stronger effect on the transversal branches. Between 5000 and 7000 K, the longitudinal branches decreases considerably. This is also clearly seen on the vDOS where the peak at high frequencies is abruptly shifted between 5000 and 7000 K, while the peak at low frequencies softens monotonously with temperature. The initial slope at low energy, from which the Debye sound velocity can be derived, strongly increases with temperature, an effect already noticed experimentally [1] but at lower temperature (from 300 to 1100 K).

As already noticed for bcc Fe [58] and for hcp Fe [13], Figure 2 demonstrates the importance of the *explicit* anharmonic effects in iron at high temperature. All the temperature effects highlighted in Fig. 2 cannot be reproduced using QHA with fixed phonon spectrum at constant volume.

From the vDOS computed at each thermodynamic point we extract the vibrational entropy $S_{\rm vib}$ and the vibrational heat capacity $C_{\rm V}$, and compare them to experimental

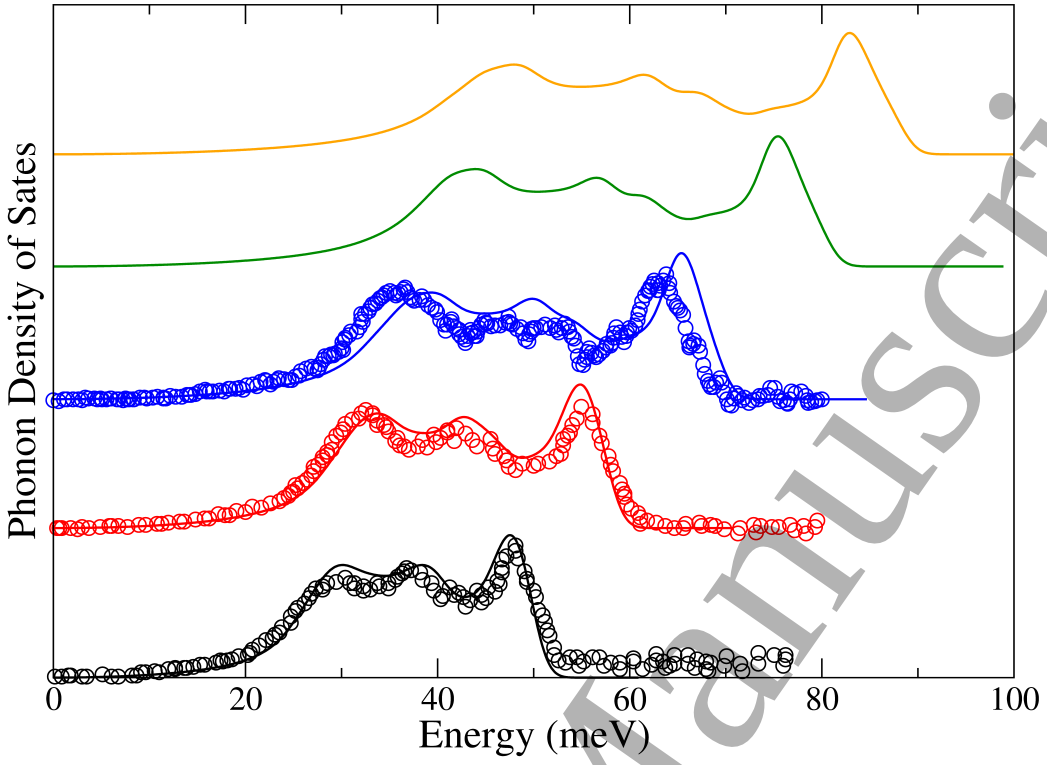

Figure 1. Room temperature phonon density of states of hcp Fe at different pressures. Straight lines: present work at 51 (black), 87 (red), 158 (blue), 245 (green) and 323 (orange) GPa. Open circles: NRIXS measurements [54, 55] at 51 (black), 85 (red) and 151 (blue) GPa.

values (see Fig. 3). Once again the agreement is really encouraging and proves the reliability of the present method. Our results for the vibrational entropy at 300 K are also in good agreement with the calculations of J. Zhuang *et al.*[59]. As shown in this work, above 1000 K, the electronic contribution to the specific heat is no longer negligible and it starts to deviate from the Dulong-Petit law.

4.2. Grüneisen parameter

The Grüneisen parameter is an important quantity for thermal EOS and to extrapolate thermophysical properties to high pressures and temperatures. It can be deduced from several measured quantities, as the vDOS [55], the atomic mean square displacements [61], Raman spectroscopy [62] or by comparing the Hugoniot and measured isentrope, as done recently at the National Ignition Facility (NIF), up to 1.4 TPa [63].

Concerning the building of equation of state (EOS), a commonly used expression for the volume dependence of the Grüneisen parameter is:

$$\gamma = \gamma_0 \left(\frac{V}{V_0}\right)^q \tag{12}$$

where γ_0 and V_0 are the Grüneisen parameter and the volume at ambient conditions,

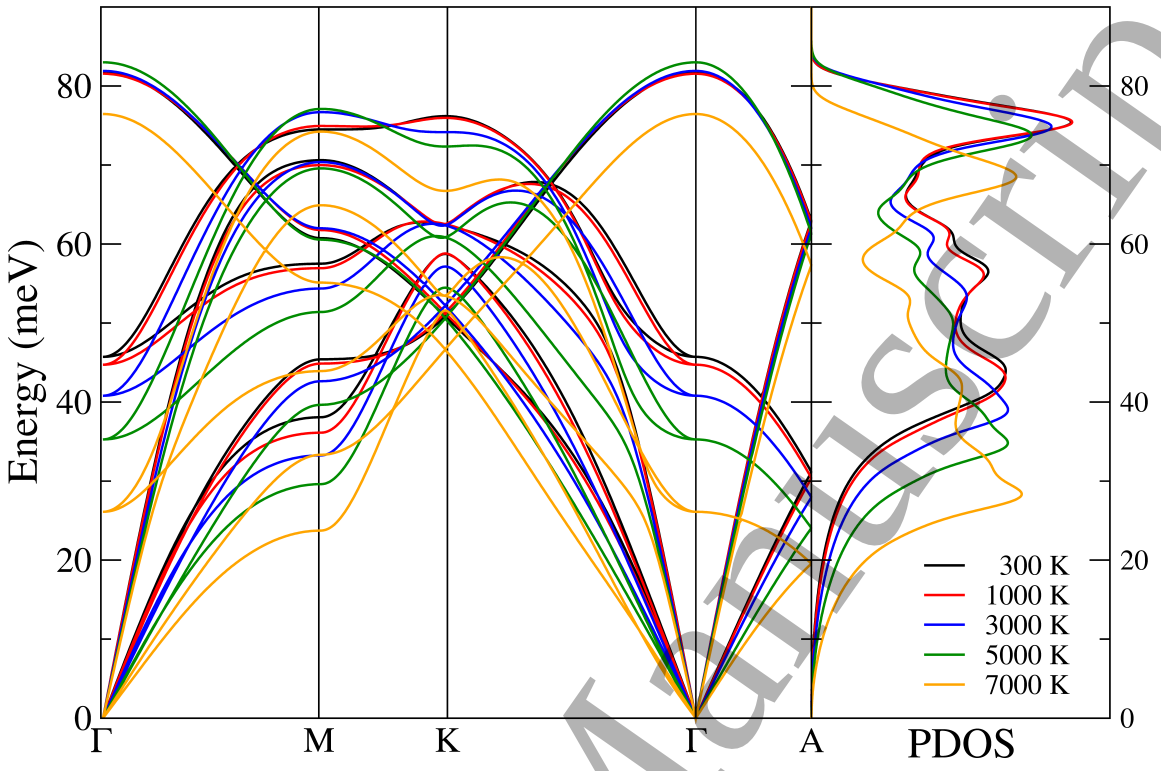

Figure 2. Temperature-dependent phonon dispersion and vDOS of hcp Fe at 300, 1000, 3000, 5000 and 7000 K at constant volume corresponding to a density of 13.06 g.cm^{-3}.

Table 1. Parameters of Eq.(12) for the variation of the Grüneisen parameter.

Reference	γ_0	q
Dubrovinsky [61]	1.78	0.69
Murphy [55]	1.88	0.8
Merkel [62]	1.68	0.7
Miozzi [17]	1.11	0.3
Present study	1.73	0.68

and q is a fitted parameter. The result of the fitting of present data with Eq. (12) is given in Table 1 in comparison with previous studies.

Present raw data at 300 K and the corresponding fitting curve are reported in Fig. 4 and compared to various experimental data and fits. Present room temperature values are in close agreement with the experimental points, specially those obtained by X-ray diffraction [61]. At high pressure, the fit also confirms the experimental constraint on the Grüneisen parameter obtained at the NIF.

The behaviour in temperature of the Grüneisen parameter is shown in Fig. 5. At the highest densities here considered (13 to 14 g.cm^{-3}), it slightly increases at low temperature then shows a strong decrease due to anharmonic effects, following the decrease observed on the phonon frequencies (see Fig. 2). At high temperatures and

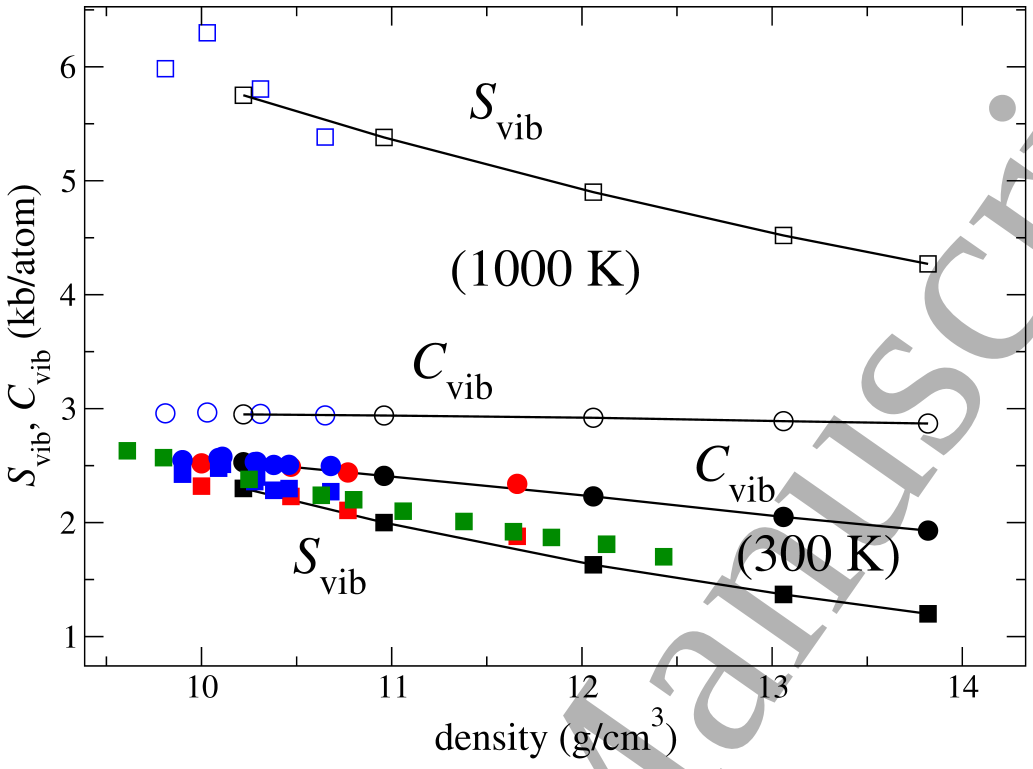

Figure 3. Vibrational entropy (squares) and vibrational heat capacity (circles) as a function of density for hcp Fe on isotherms T = 300 K (filled symbols) and 1000 K (opened symbols). Present work and NRIXS measurements [60, 54, 1]] are respectively in black, green, red and blue.

densities, the Grüneisen parameter is almost constant, as already observed by Alfè *et al.* [13]. At 6000 K, they obtain a constant value of 1.45, while at 7000 K we have around 1.0. Since here we only calculate the vibrational contribution, we can estimate the electronic part around 0.3-0.4 at temperatures and densities relevant for the Earth's core.

4.3. Thermal expansion

As mentioned in section 3, the thermal expansion matrix can be calculated using the third order effective IFCs. For an hcp crystal, there is two coefficients of thermal expansion (CTE), one for the basal plane (α_a) and a second one for the perpendicular direction along the c axis (α_c), while the volumetric CTE is given by $\alpha_V = 2\alpha_a + \alpha_c$. Present results at 300 K are presented in Fig. 6 and compared to the volumetric CTE deduced from the experimental vDOS obtained with NRIXS [60]. As for the vDOS and the vibrational entropy, the agreement is excellent. We observe an anisotropy between the thermal expansion along the a and c axis, α_c being larger than α_a. Therefore the c/a ratio increases with temperature as found in previous theoretical [65, 66] and experimental studies [67, 68]. This anisotropy decreases at core density where α_a and α_c are close to each other at 300 K [69].

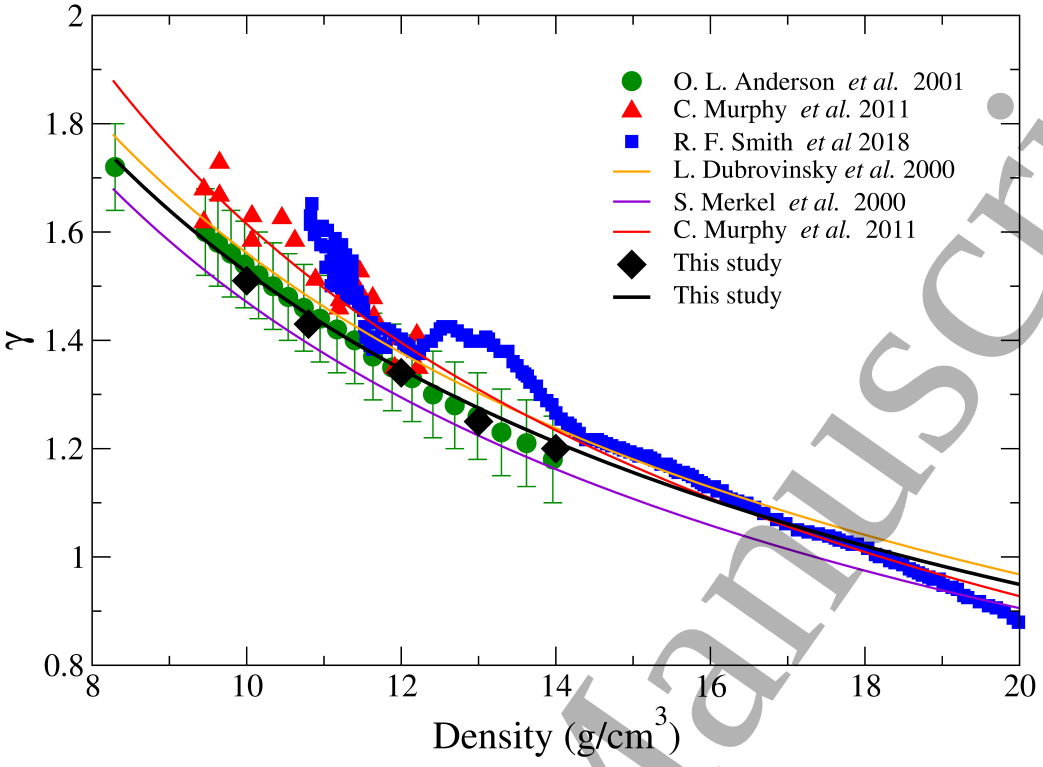

Figure 4. Grüneisen parameter of hcp Fe at T = 300 K as a function of density. The black diamonds are the results of present calculations. The green circles, the red triangles and the blue squares are experimental data from Ref. [55, 64, 63] respectively. The black, orange, violet and green lines are fits following Eq. (12) for present data and Ref. [61, 62, 55].

The effect of temperature on the volutmetric CTE is presented in Fig. 7. It increases between 300 and 1000 K due to the filling of the phonon energy levels, then decreases at higher temperatures due to anharmonic effects (a trend similar to the one observed for the Grüneisen parameter, according to Eq. (8)). At 5000 K, we slightly underestimate the experimental value of Duffy and Ahrens [69], possibly because of the electronic contribution. In present calculations we also observe that the anisotropy between the basal plane and the c axis decreases with temperature so the c/a ratio stays below the ideal value of 1.633 in agreement with Gannarelli *et al.* [66].

5. Elastic properties and sound velocities

5.1. Comparison with previous ab initio calculations at 0 K

In Fig. 8, we compare present compressional and shear velocities for hcp-Fe at 0 K to previous *ab initio* calculations with different methods: PAW [8, 53, 10], ultrasoft pseudopotentials [11] or all-electrons methods [52, 12, 70]. All these calculations use the GGA functional to describe the exchange-correlation energy and potential. As expected, the agreement between all these results is really good. The discrepancies

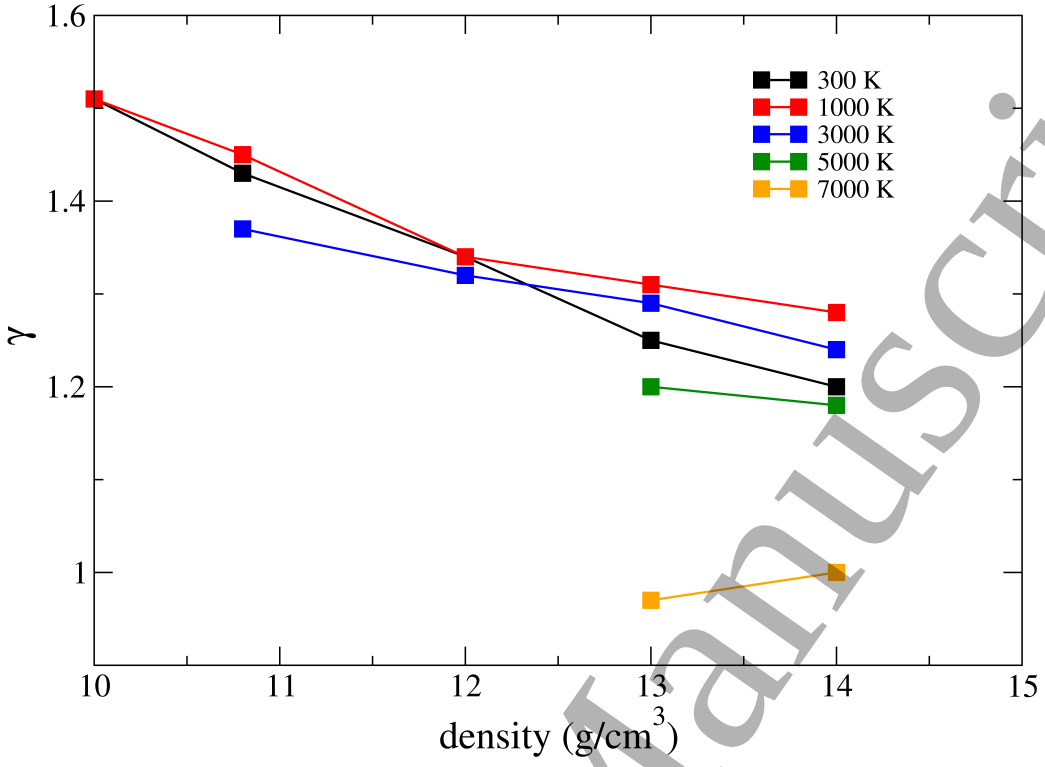

Figure 5. Grüneisen parameter of hcp Fe as a function of density and temperature.

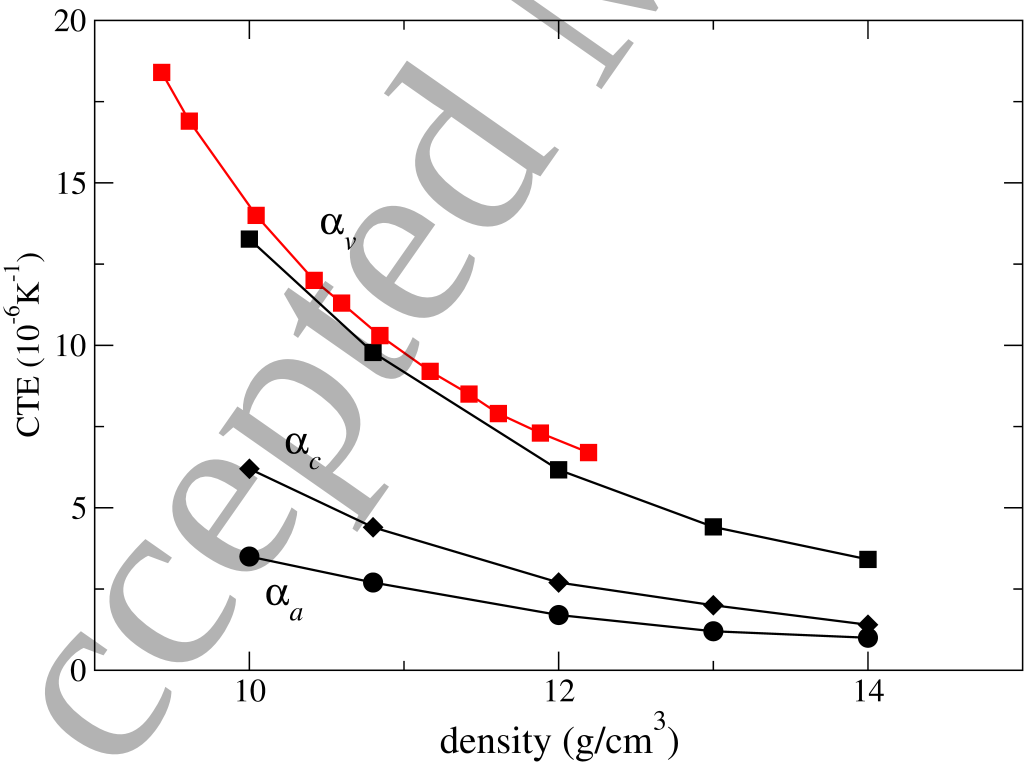

Figure 6. CTE of hcp Fe at T = 300 K as a function of density. α_V is the volumetric thermal expansion while α_a and α_c are the linear coefficient in the x (y) and z direction respectively. The black symbols are the results of the calculation while the red squares are the data extracted from the NRIXS measurements [60].

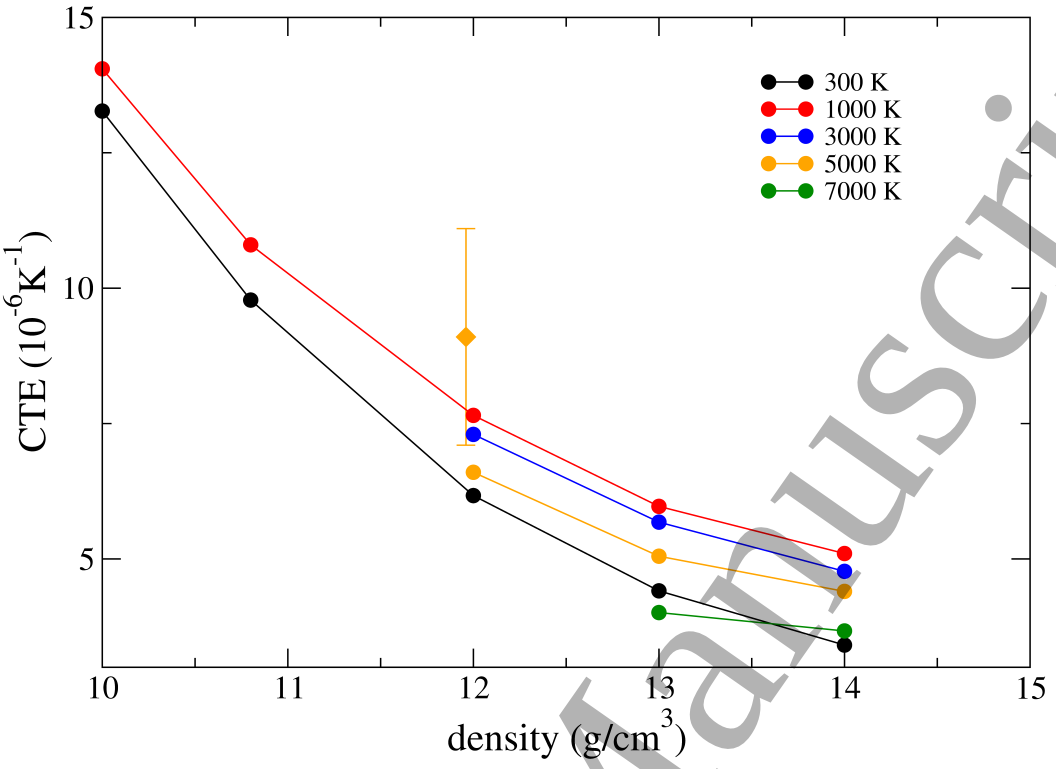

Figure 7. Temperature dependence of the volumetric CTE as a function of density. The orange diamonds with error bar is the experimental value of Duffy and Ahrens [69] at $T = 5200 \pm 500$ K.

observed with the PAW calculations of Vočadlo *et al.* [8] (filled red squares in Fig. 8) are certainly due to a less dense **k**-points grid or a smaller number of valence electrons. Their more recent results [10, 53] (open red squares in Fig. 8) are in better agreement with other calculations. We also observe large discrepancies with the data of Sha and Cohen [12] (filled orange down triangles in Fig. 8) obtained using full-potential linear-muffin-tin-orbital (FPLMTO) calculations. This is unexpected and seems incoherent with calculations using full charge density exact muffin-tin orbital (FCD-EMTO) method [71, 70]. The difference increasing with density, it is possible that a too large muffin-tin radius was used in the work of Sha and Cohen, resulting in an overlap between the spheres around each ion and a smaller pressure than expected. This would explain why their compression curve strongly diverges from the experimental one at low volumes (see the figure 4.e of Ref. [72]). If we put aside these two works [8, 12], we observe a linear dependence on density for the sound velocities, with differences below 2% between the calculations, confirming the validity of the Birch's law for athermal calculations (i.e. the validity of the quasi-harmonic approximation).

5.2. Comparison with experimental data at 300 K

We compare present theoretical velocities to the experimental data on Fig. 9. Two main techniques are used to obtain the velocities: the NRIXS and the inelastic X-Ray

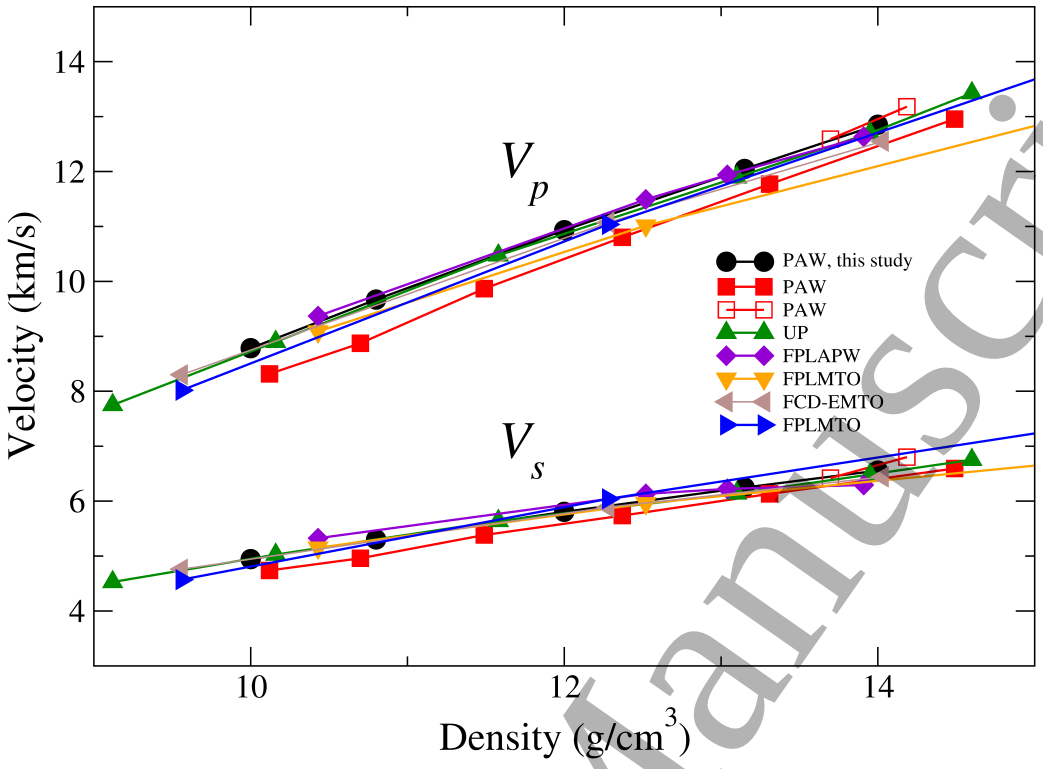

Figure 8. Theoretical compressional V_P and shear V_S velocities for hcp-Fe. Black circles, PAW, this study; red squares, PAW, Ref. [8]; open red squares, PAW, Ref. [53, 10]; green triangles, ultrasoft pseudopotentials, Ref. [11]; violet diamonds, FPLAW, Ref. [52]; orange down triangles, FPLMTO, Ref. [12]; brown left triangles, FCD-EMTO Ref. [70]; blue right triangles, FPLMTO, Ref. [71].

scattering (IXS), with different drawbacks and advantages. Basically NRIXS is more reliable to provide V_S than V_P while for IXS it is the opposite. For a complete discussion and a comparison of these techniques, see Ref. [2], which also provides a fit to combined data sets available in literature, aslo including results by impulsive stimulated light scattering[73] and picosecond acoustics[74].

Clearly, the theoretical results overestimate the experimental velocities for the low densities, but the difference diminishes at higher densities. For V_P, at 10 g.cm^{-3}, we have a difference of about 8 % with the fit of Ref. [2], which drops to 2 % at 13 g.cm^{-3} if we extrapolate the experimental data. The comparison is worse with the sub-linear relation proposed by Mao *et al.* [75] at core densities with differences up to 8%. The difference with the NRIXS measurements is larger, about 12 % from 10 to 12.5 g.cm^{-3}. For V_S, the situation is even worse, with differences going from 18 to 12% respectively at 10 and 13 g.cm^{-3}.

Can we understand these discrepancies and the reasons behind, and more, can we propose a way to correct them? To answer these questions, we need to turn to the comparison between the experimental and *ab initio* EOS of iron. Fortunately, the EOS obtained with the PAW atomic datasets that we use here have been extensively compared with the more recent EOS derived from diamond anvil cell data [77, 45, 72, 16],

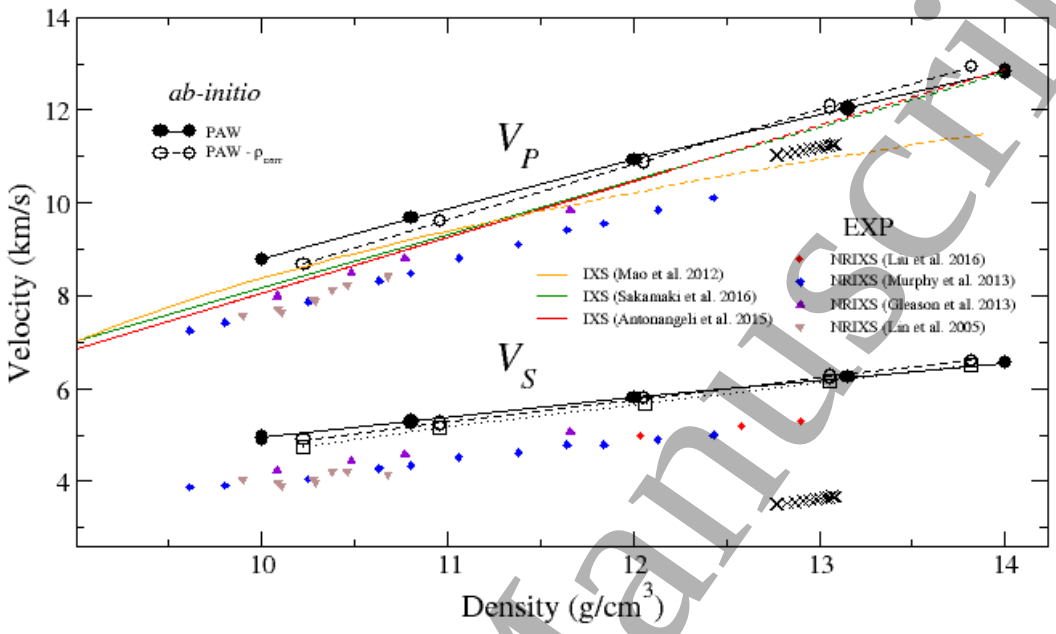

Figure 9. Comparison with experimental compressional V_P and shear V_S velocities for hcp-Fe. Theory: black circles, PAW, this study (same as in Fig. 8); open circles, PAW with corrected pressure. Experiments: red line, linear fit of combined datasets, Ref. [2]; green line, linear fit of IXS data, Ref. [3]; orange line, power law fit of IXS, Ref [75]; red circles, blue diamonds, violet triangles and brown down triangles, NRIXS measurements of Ref. [76], [60], [54], and [1] respectively. PREM is shown as crosses. For the fits, the lines cover the data points while the dashed ones are extrapolations.

either using Vinet or Birch–Murnaghan EOS. These comparisons bring out a number of important points. Below 200 GPa, the *ab initio* EOS underestimates the experimental pressure, while above the pressure is overestimated. Dewaele *et al.* [45] also emphasize an overestimation of the bulk modulus with the filling of the *d*-orbitals due to the GGA approximation itself. In conclusion they propose a procedure to correct the *ab initio* EOS (i) by using the experimental equilibrium volume instead of the theoretical one, and (ii) by using the K_T and K'_T recalculated at this volume.

In the same spirit we can try to correct present theoretical sound velocities. First, using the theoretical and experimental parameters of the Vinet EOS, we have corrected present densities to obtain the experimental pressure (see the open circles in Fig. 9). As direct consequence of this correction, velocities are decreased for densities lower than 12.5 g.cm^{-3} (the density where both EOS give the same pressure) and increased above. The effect is significant for V_P and improve the agreement with experiments but is almost negligible for V_S due to a weaker slope. Interestingly this correction gives a density dependence of the compressional velocity in close agreement with the fit proposed by Antonageli *et al* [2] and Sakamaki *et al* [3] with a constant overestimation

of the compressional velocities around 4% between 10 and 14 g.cm^{-3}.

Once the pressure correction performed, the discrepancies that we still observe for the shear velocity can only be explained by an overestimation of the shear modulus G in the calculations. If we compare the K_T obtained with present athermal calculations and the values taken from the EOS of Sakai *et al.* the difference is around 9% for the range of densities considered here. An increase of G around 20 % would be needed to find a good agreement with experiments for both velocities.

The second correction that can be made to the theoretical results comes from the temperature difference between calculations and experiments, (0 K vs. 300 K). In the results presented in the next section we have included the velocities that we obtain at room temperature. This correction lowers the velocities, with a larger effect for V_S, but is still not sufficient to explain the discrepancies.

5.3. Temperature dependence of the sound velocities

5.3.1. Results and Birch's law We present the temperature dependence of the compressional and shear velocities of hcp iron on Fig. 10. To calculate K_S we use the thermal expansion α and the Grüneisen parameter γ obtained using Eq. (8) and (3) (see sections 4.3 and 4.2). Both velocities decrease with temperature but V_S much more rapidly than V_P. This is simply due to the fact that C_{11} and C_{33} decrease with temperature while C_{12} and C_{13} increase. So, according to equation (6), these effects compensate each other for K_T while they amplify each other for G. The temperature effects on velocities weaken as the denity increase.

We fit these data using the formula proposed by Sakamaki *et al.* [3]:

$$V(\rho, T) = M\rho + B + A(\rho - \rho^*)T \tag{13}$$

where M and B are the coefficient of Birch's law at 0 K while A and ρ^* give the temperature dependence of the velocities. In equation (13), T is in K, density in g.cm^{-3} and V in kms^{-1}. In the present fit, we discard the data at $\rho = 10.22$ g.cm^{-3} and 3000 K since at these thermodynamic conditions iron is either liquid or fcc [78]. For V_P we found $M = 1.20$, $B = -3.66$, $A = 4.55 \times 10^{-5}$ and $\rho^* = 15.68$ g.cm^{-3}. For V_S we found $M = 0.50$, $B = -0.36$, $A = 5.24 \times 10^{-5}$ $\rho^* = 19.6$ g.cm^{-3}. We plot in Fig. 11 a comparison between the results of the present fit and the direct calculation of the velocities. The differences do not exceed 2 % and are larger for V_S than for V_P. We therefore conclude that for the range of densities considered here, and up to 7000 K, velocities along an isotherm linearly depend on density and that it is not necessary to introduce a power law function for V_P as proposed in Ref. [75]. As expected the temperature effects are more important at low densities and tends to reduce at the inner core boundary (ICB) but since the melting temperature is much higher they cannot be neglected.

5.3.2. Comparison with previous theoretical work At 12.52 g.cm^{-3}, when the temperature increases, Sha and Cohen [12] obtain a reduction of the compressional

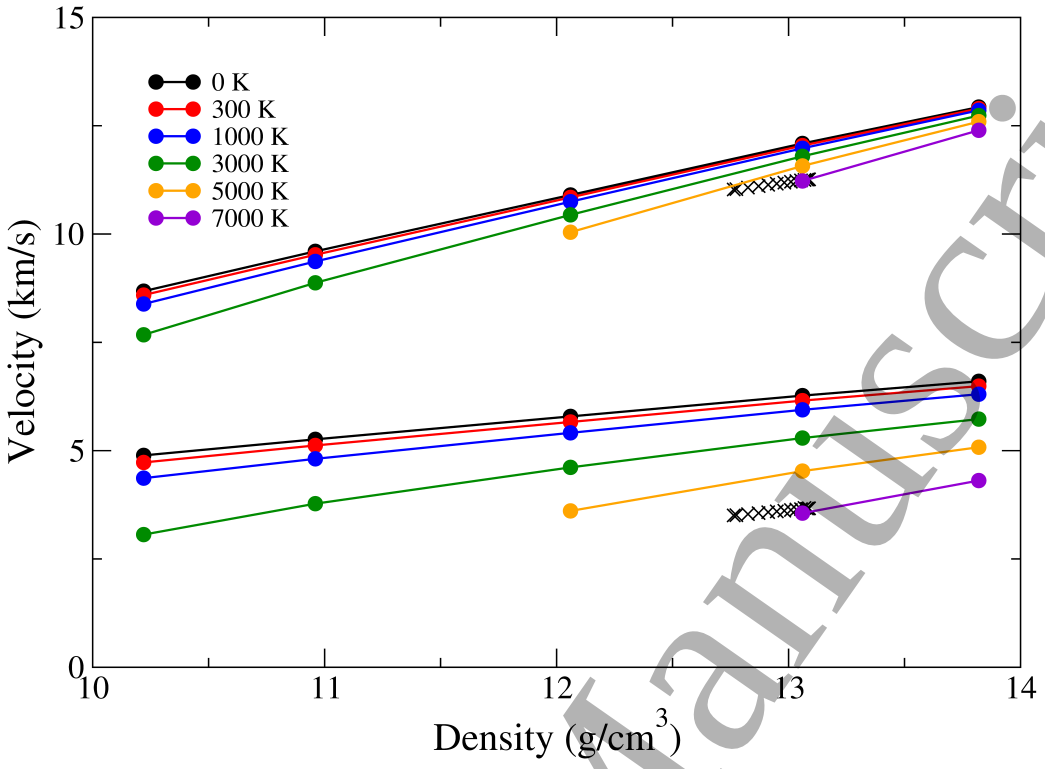

Figure 10. Compressional V_P and shear V_S velocities for hcp-Fe at 0 (black), 300 (red), 1000 (blue), 3000 (green), 5000 (orange) and 7000 K (violet) as a function of density. The compressional and shear velocity of the PREM [6] inner core are shown as large crosses.

velocity equal to 0.13 m.s^{-1}.K^{-1}, which is comparable to the present value of 0.15 m.s^{-1}.K^{-1}. The difference in the case of V_S is larger, they found 0.35 m.s^{-1}.K^{-1} to be compared with present value of 0.39 m.s^{-1} K^{-1}. At 10.43 g.cm^{-3}, they obtain a value around 0.09 m.s^{-1}.K^{-1} for V_P, much lower than present result 0.27 m.s^{-1}.K^{-1}. This difference is certainly due to anharmonic effects beyond the thermal expansion and not taken into account by the quasi harmonic approximation. On an isotherm, these anharmonic terms are supposed to be more important at low densities and this would explain these discrepancies.

We use the (ρ, T) values of Refs. [53, 10] in the present fit (see Eq. (13)) to compare their sound velocities values with present results (see Fig. 12). The agreement is really good, all the more so when considering that the correction on present densities (coming from the discrepancy between the theoretical and experimental EOS) is not taken into account in these previous studies.

However we observe larger differences at high temperature. Elastic properties are difficult to obtain at temperatures close to the melting point. For example at 13 g.cm^{-3} and 7200 K, we observe a distorsion in the hcp supercell. A plane of atoms slides along the [010] direction and the hcp structure is no longer stable. This is expected to have a strong impact on the values of the elastic constants which can considerably

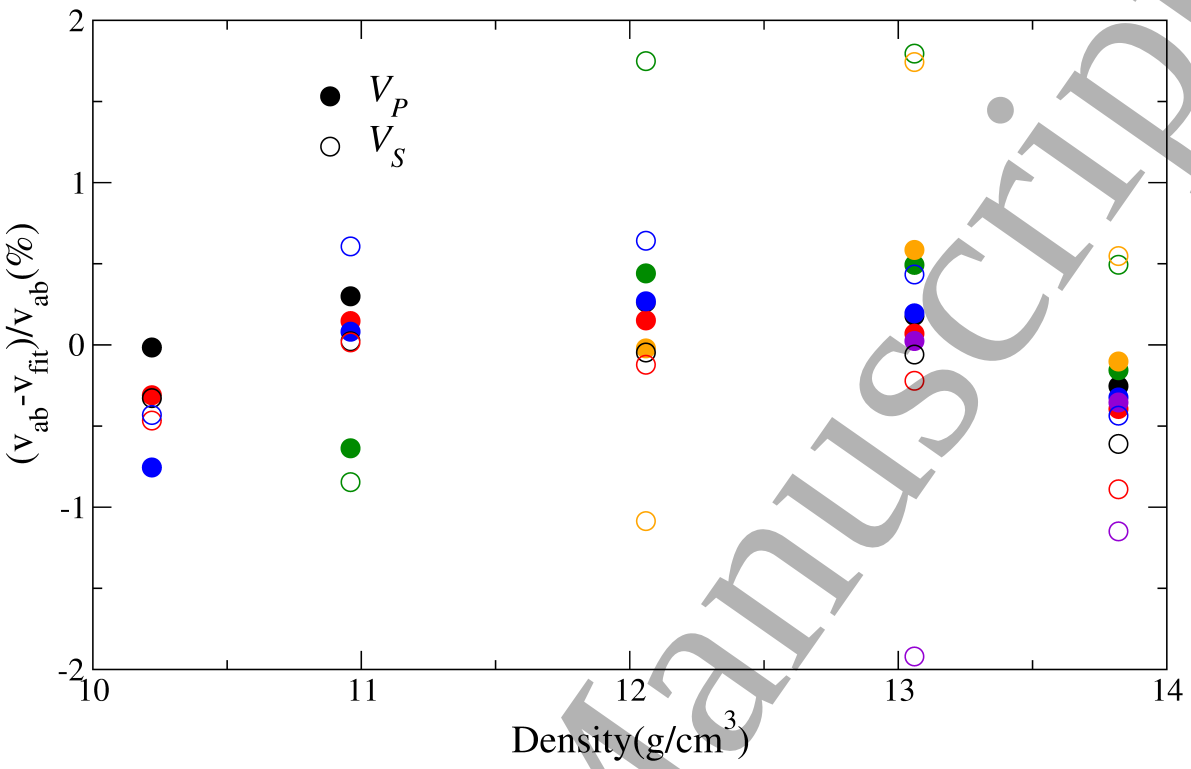

Figure 11. Comparison between the compressional (filled circles) and shear (open circles) velocities obtained form the AIMD and from the fit (see Eq. (13)). The colors of the temperatures are the same as in Figure 10.

drop. Unfortunately these phenomena are related to the size of the supercell, and the conclusions from those simulations are limited. It could be premelting effect, but also a transition towards another solid structure as bcc which could be more stable than the hcp structure at temperatures close to the melting point[79]. Martorell *et al.* [10] observed the same phenomena but on smaller supercells (64 atoms compared to 180 atoms in present simulations). A deformation of the supercell as used in this work to calculate the elastic constants could also induce sliding planes. We believe that these results should be treated with caution.

5.3.3. Comparison with experimental data If temperature effects on the sound velocities of iron have been calculated for thermodynamic conditions corresponding to those expected at the inner-core, outer-core boundary (ICB) [12, 53, 10], results of calculations have never been directly compared to experimental measurements at the actual density and temperature where data have been collected (i.e. at lower densities and temperature). V_P has been much more studied and we are aware of only one NRIXS experiment to measure V_S up to 1700 K [1]. The temperature dependence deduced from the experiments for V_P are in open disagreement. Lin *et al.* [1] using NRIXS estimated a temperature decrease of about 0.35 m.s^{-1}.K^{-1} at a constant density value of 10.25 g.cm^{-3}. For the same density and temperature from 300 to 700 K, Mao *et al.* [75]

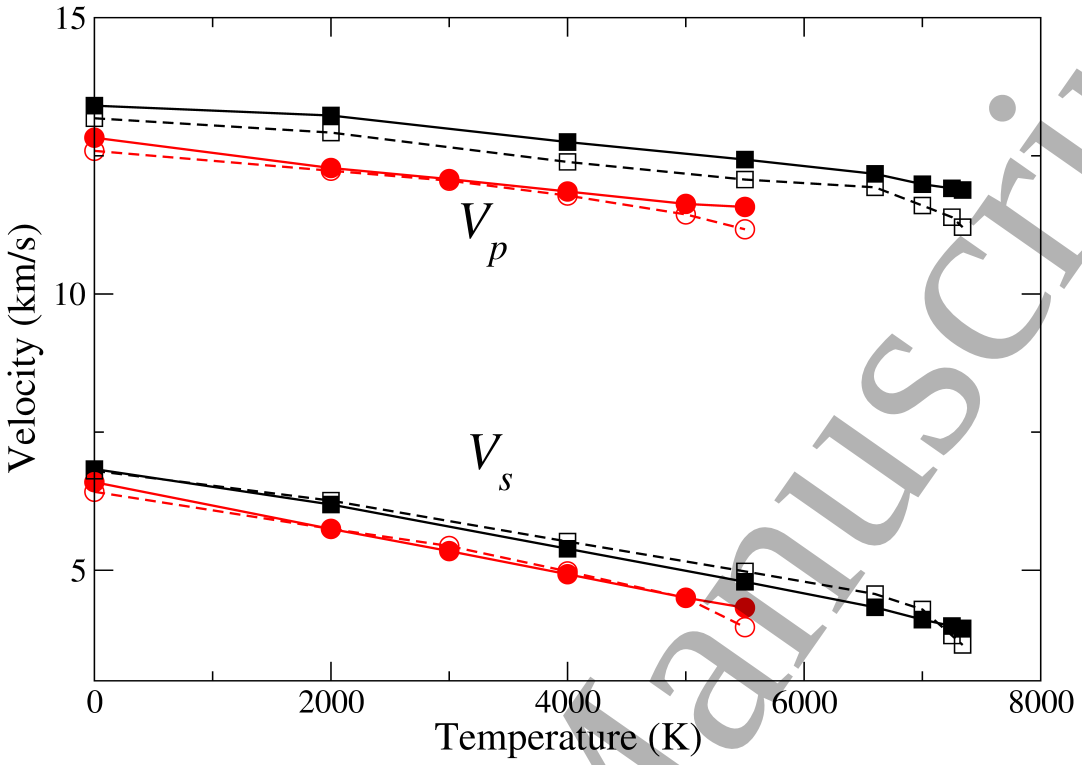

Figure 12. Comparison between the sound velocities obtained with the present fit (filled symbols) and the values obtained in Refs. [53] (open red circles) and Refs. [10] (open black squares).

using IXS give a value almost two times larger: 0.67 m.s^{-1}.K^{-1}. From the fit proposed by Sakamaki *et al.* [3] based on their IXS measurements, we obtain a value of 0.28 m.s^{-1}.K^{-1} at this density. In contrast, Antonangeli *et al.* [80] and Ohtani *et al.* [81], starting with IXS reported the temperature effects to be negligible up to 1000 K.

From Eq. (13) we find a value of 0.28 m.s^{-1}.K^{-1}, in agreement with Sakamaki *et al.* [3] and we do not support the large value found by Mao *et al.* [75]. The agreement remains very good at high pressure and temperature. They predict a value of 11.85 km.s^{-1} at 330 GPa, 5500 K) while we obtain 11.93 km.s^{-1}. For V_S, Lin *et al.* [1] using NRIXS estimated a temperature decrease of about 0.46 m.s^{-1}. For the same density, Eq. (13) gives a similar value.

6. Conclusion

Using a new method to calculate the vibrational contribution to the free energy we have studied the temperature dependence of physical quantities of hcp iron up to the Earth's core conditions. To assess the validity of the present approach we first compare the results obtained to recent experimental data in the (P, T) domain accessible to experiments. We obtain an excellent agreement between present calculations of the phonon density of states at room temperature and NRIXS measurements which gives

weight to subsequent predictions at temperatures not reached in experiments. The Grüneisen parameter and the coefficients of thermal expansion are also well reproduced by present calculations at room temperature. We also show that the underestimation of the iron densities by GGA is partially responsible for the discrepancies observed between experimental and theoretical compressional sound velocities. Overall, the agreement is better with IXS measurements than with NRIXS. Following a recent experimental work, we also provide the parameters of a high-temperature Birch's law for hcp-Fe. In the future, we hope that present data can be used to build reliable EOS of iron for Earth and planetary models.

7. Acknowledgements

We would like to thank M. Torrent for helpful discussions. This research was supported by the PlanetLab program of the Agence Nationale de la Recherche (ANR) grant ANR-12-BS04-0015-04.

References

[1] Lin J F, Sturhahn W, Zhao J, Shen G, kwang Mao H and Hemley R J 2005 *Science* **308** 1892–1894
[2] Antonangeli D and Ohtani E 2015 *Prog. in Earth and Planet. Sci.* **2** 3
[3] Sakamaki T, Ohtani E, Fukui H, Kamada S, Takahashi S, Sakairi T, Takahata A, Sakai T, Tsutsui S, Ishikawa D, Shiraishi R, Seto Y, Tsuchiya T and Baron A Q R 2016 *Science Advances* **2** e1500802
[4] Antonangeli D, Morard G, Paolasini L, Garbarino G, Murphy C A, Edmund E, Decremps F, Fiquet G, Bosak A, Mezouar M and Fei Y 2018 *Earth and Planetary Science Letters* **482** 446–453
[5] Edmund E, Antonangeli D, Decremps F, Miozzi F, Morard G, Boulard E, Clark A, Ayrinhac S, Gauthier M, Morand M and Mezouar M 2019 *Journal of Geophysical Research : Solid Earth* **124** 3436–3447
[6] Dziewonski A M and Anderson D L 1981 *Physics of the Earth and Planetary Interiors* **25** 297–356
[7] Kennett B L N, Engdahl E R and Buland R 1995 *Geophysical Journal International* **122** 108–124
[8] Vočadlo L, Alfè D, Gillan M and Price G 2003 *Physics of the Earth and Planetary Interiors* **140** 101–125 geophysical and Geochemical Evolution of the Deep Earth
[9] Vočadlo L 2007 *Earth and Planetary Science Letters* **254** 227–232
[10] Martorell B, Brodholt J, Wood I G and Vočadlo L 2013 *Earth and Planetary Science Letters* **365** 143–151
[11] Tsuchiya T and Fujibuchi M 2009 *Physics of the Earth and Planetary Interiors* **174** 212–219 advances in High Pressure Mineral Physics: from Deep Mantle to the Core
[12] Sha X and Cohen R E 2010 *Geophysical Research Letters* **37** L10302
[13] Alfè D, Price G D and Gillan M J 2001 *Phys. Rev. B* **64**(4) 045123
[14] Sha X and Cohen R E 2010 *Phys. Rev. B* **81**(9) 094105
[15] Bouchet J, Mazevet S, Morard G, Guyot F and Musella R 2013 *Phys. Rev. B* **87**(9) 094102
[16] Fei Y, Murphy C, Shibazaki Y, Shahar A and Huang H 2016 *Geophysical Research Letters* **43** 6837–6843
[17] Miozzi F, Matas J, Guignot N, Badro J, Siebert J and Fiquet G 2020 *Minerals* **10**
[18] Fultz B 2010 *Progress in Materials Science* **55** 247–352
[19] Giura P, Paulatto L, He F, Lobo R P S M, Bosak A, Calandrini E, Paolasini L and Antonangeli D 2019 *Phys. Rev. B* **99**(22) 220304

[20] Calandrini E, Paulatto L, Antonangeli D, He F, Lobo R P S M, Capitani F, Brubach J B, Roy P, Vincent L and Giura P 2021 *Phys. Rev. B* **103**(5) 054302

[21] Glensk A, Grabowski B, Hickel T and Neugebauer J 2015 *Phys. Rev. Lett.* **114**(19) 195901

[22] Souvatzis P, Eriksson O, Katsnelson M I and Rudin S P 2008 *Phys. Rev. Lett.* **100**(9) 095901

[23] Errea I, Calandra M and Mauri F 2013 *Phys. Rev. Lett.* **111**(17) 177002

[24] Errea I, Calandra M and Mauri F 2014 *Phys. Rev. B* **89**(6) 064302

[25] Hellman O, Abrikosov I A and Simak S I 2011 *Phys. Rev. B* **84**(18) 180301

[26] Hellman O, Steneteg P, Abrikosov I A and Simak S I 2013 *Phys. Rev. B* **87**(10) 104111

[27] Bottin F, Bieder J and Bouchet J 2020 *Computer Physics Communications* **254** 107301

[28] Tadano T, Gohda Y and Tsuneyuki S 2014 *Journal of Physics: Condensed Matter* **26** 225402

[29] Nelson L J, Hart G L W, Zhou F and Ozoliņš V 2013 *Phys. Rev. B* **87**(3) 035125

[30] Gong Y, Grabowski B, Glensk A, Körmann F, Neugebauer J and Reed R C 2018 *Phys. Rev. B* **97**(21) 214106

[31] Esfarjani K and Stokes H T 2008 *Phys. Rev. B* **77**(14) 144112

[32] Bouchet J, Bottin F, Recoules V, Remus F, Morard G, Bolis R M and Benuzzi-Mounaix A 2019 *Phys. Rev. B* **99**(9) 094113

[33] Shulumba N, Hellman O, Rogström L, Raza Z, Tasnádi F, Abrikosov I A and Odén M 2015 *Applied Physics Letters* **107** 231901

[34] Kim D S, Hellman O, Shulumba N, Saunders C N, Lin J Y Y, Smith H L, Herriman J E, Niedziela J L, Abernathy D L, Li C W and Fultz B 2020 *Phys. Rev. B* **102**(17) 174311

[35] Troyan I A, Semenok D V, Kvashnin A G, Sadakov A V, Sobolevskiy O A, Pudalov V M, Ivanova A G, Prakapenka V B, Greenberg E, Gavriliuk A G, Lyubutin I S, Struzhkin V V, Bergara A, Errea I, Bianco R, Calandra M, Mauri F, Monacelli L, Akashi R and Oganov A R 2021 *Advanced Materials* **33** 2006832

[36] Esfarjani K, Chen G and Stokes H T 2011 *Phys. Rev. B* **84**(8) 085204

[37] The ABINIT code is a common project of the Catholic University of Louvain (Belgium), Corning Incorporated, CEA (France) and other collaborators (URL http://www.abinit.org).

[38] Gonze X, Amadon B, Antonius G, Arnardi F, Baguet L, Beuken J M, Bieder J, Bottin F, Bouchet J, Bousquet E, Brouwer N, Bruneval F, Brunin G, Cavignac T, Charraud J B, Chen W, Côté M, Cottenier S, Denier J, Geneste G, Ghosez P, Giantomassi M, Gillet Y, Gingras O, Hamann D R, Hautier G, He X, Helbig N, Holzwarth N, Jia Y, Jollet F, Lafargue-Dit-Hauret W, Lejaeghere K, Marques M A, Martin A, Martins C, Miranda H P, Naccarato F, Persson K, Petretto G, Planes V, Pouillon Y, Prokhorenko S, Ricci F, Rignanese G M, Romero A H, Schmitt M M, Torrent M, van Setten M J, Troeye B V, Verstraete M J, Zérah G and Zwanziger J W 2020 *Computer Physics Communications* **248** 107042

[39] Romero A H, Allan D C, Amadon B, Antonius G, Applencourt T, Baguet L, Bieder J, Bottin F, Bouchet J, Bousquet E, Bruneval F, Brunin G, Caliste D, Côté M, Denier J, Dreyer C, Ghosez P, Giantomassi M, Gillet Y, Gingras O, Hamann D R, Hautier G, Jollet F, Jomard G, Martin A, Miranda H P C, Naccarato F, Petretto G, Pike N A, Planes V, Prokhorenko S, Rangel T, Ricci F, Rignanese G M, Royo M, Stengel M, Torrent M, van Setten M J, Van Troeye B, Verstraete M J, Wiktor J, Zwanziger J W and Gonze X 2020 *The Journal of Chemical Physics* **152** 124102

[40] Blöchl P E 1994 *Phys. Rev. B* **50**(24) 17953–17979

[41] Torrent M, Jollet F, Bottin F, Zérah G and Gonze X 2008 *Computational Materials Science* **42** 337–351

[42] Perdew J P, Burke K and Ernzerhof M 1996 *Phys. Rev. Lett.* **77**(18) 3865–3868

[43] Holzwarth N, Tackett A and Matthews G 2001 *Computer Physics Communications* **135**

329–347
[44] ATOMPAW is a general license public code developed at Wake Forest University. Some of its capabilities have been developed at the Commissariat à l'énergie atomique (http://pwpaw.wfu.edu).
[45] Dewaele A, Torrent M, Loubeyre P and Mezouar M 2008 *Phys. Rev. B* **78**(10) 104102
[46] Bottin F, Leroux S, Knyazev A and Zérah G 2008 *Computational Materials Science* **42** 329–336
[47] Bouchet J and Bottin F 2015 *Phys. Rev. B* **92**(17) 174108
[48] Anderson O L 2000 *Geophysical Journal International* **143** 279–294
[49] Stacey F D 2005 *Reports on Progress in Physics* **68** 341–383
[50] Leibfried G and Ludwig W 1961 Theory of anharmonic effects in crystals (*Solid State Physics* vol 12) ed Seitz F and Turnbull D (Academic Press) pp 275–444
[51] Wallace D 1998 *Thermodynamics of Crystals* Dover books on physics (Dover Publications) ISBN 9780486402123
[52] Steinle-Neumann G, Stixrude L and Cohen R E 1999 *Phys. Rev. B* **60**(2) 791–799
[53] Vočadlo L, Dobson D P and Wood I G 2009 *Earth and Planetary Science Letters* **288** 534–538
[54] Gleason A E, Mao W L and Zhao J Y 2013 *Geophysical Research Letters* **40** 2983–2987
[55] Murphy C A, Jackson J M, Sturhahn W and Chen B 2011 *Physics of the Earth and Planetary Interiors* **188** 114–120
[56] Alfè D 2009 *Phys. Rev. B* **79**(6) 060101
[57] Sola E and Alfè D 2009 *Phys. Rev. Lett.* **103**(7) 078501
[58] Luo W, Johansson B, Eriksson O, Arapan S, Souvatzis P, Katsnelson M I and Ahuja R 2010 *Proceedings of the National Academy of Sciences* **107** 9962–9964
[59] Zhuang J, Wang H, Zhang Q and Wentzcovitch R M 2021 *Physical Review B* **103** 144102 publisher: American Physical Society
[60] Murphy C A, Jackson J M and Sturhahn W 2013 *Journal of Geophysical Research: Solid Earth* **118** 1999–2016
[61] Dubrovinsky L, Saxena S, Dubrovinskaia N, Rekhi S and Le Bihan T 2000 *American Mineralogist* **85** 386–389
[62] Merkel S, Goncharov A F, kwang Mao H, Gillet P and Hemley R J 2000 *Science* **288** 1626–1629
[63] Smith R F, Fratanduono D E, Braun D G, Duffy T S, Wicks J K, Celliers P M, Ali S J, nella A F P, Kraus R G, Swift D C, Collins G W and Eggert J H 2018 *Nat. Astron.* **2** 452
[64] Anderson O L, Dubrovinsky L, Saxena S K and LeBihan T 2001 *Geophysical Research Letters* **28** 399–402
[65] Moustafa S G, Schultz A J, Zurek E and Kofke D A 2017 *Phys. Rev. B* **96**(1) 014117
[66] Gannarelli C S, Alfè D and Gillan M 2005 *Physics of the Earth and Planetary Interiors* **152** 67–77
[67] Sakai T, Ohtani E, Hirao N and Ohishi Y 2011 *Geophysical Research Letters* **38**
[68] Fischer R A and Campbell A J 2015 *American Mineralogist* **100** 2718–2724
[69] Duffy T S and Ahrens T J 1993 *Geophysical Research Letters* **20** 1103–1106
[70] Kádas K, Vitos L and Ahuja R 2008 *Earth and Planetary Science Letters* **271** 221–225
[71] Söderlind P, Moriarty J A and Wills J M 1996 *Phys. Rev. B* **53**(21) 14063–14072
[72] Sakai T, Takahashi S, Nishitani N, Mashino I, Ohtani E and Hirao N 2014 *Physics of the Earth and Planetary Interiors* **228** 114–126 high-Pressure Research in Earth Science: Crust, Mantle, and Core

[73] Crowhurst J, Goncharov A and Zaug J 2004 *Journal of Physics: Condensed Matter* **16** S1137
[74] Decremps F, Antonangeli D, Gauthier M, Ayrinhac S, Morand M, Marchand G L, Bergame F and Philippe J 2014 *Geophysical Research Letters* **41** 1459–1464
[75] Mao Z, Lin J F, Liu J, Alatas A, Gao L, Zhao J and Mao H K 2012 *Proceedings of the National Academy of Sciences* **109** 10239–10244
[76] Liu J, Lin J F, Alatas A, Hu M Y, Zhao J and Dubrovinsky L 2016 *Journal of Geophysical Research: Solid Earth* **121** 610–623
[77] Dewaele A, Loubeyre P, Occelli F, Mezouar M, Dorogokupets P I and Torrent M 2006 *Phys. Rev. Lett.* **97**(21) 215504
[78] Anzellini S, Dewaele A, Mezouar M, Loubeyre P and Morard G 2013 *Science* **340** 464–466
[79] Belonoshko A B, Fu J and Smirnov G 2021 *Phys. Rev. B* **104**(10) 104103
[80] Antonangeli D, Komabayashi T, Occelli F, Borissenko E, Walters A C, Fiquet G and Fei Y 2012 *Earth and Planetary Science Letters* **331-332** 210–214
[81] Ohtani E, Shibazaki Y, Sakai T, Mibe K, Fukui H, Kamada S, Sakamaki T, Seto Y, Tsutsui S and Baron A Q R 2013 *Geophysical Research Letters* **40** 5089–5094